Assessment of the SEDE Model: Determination of Membrane Potential and Salt Rejection of a Nanofiltration Membrane

Yannick Lanteri[1], Anthony Szymczyk[2], Sébastien Déon[1] and Patrick Fievet[1,*]

[1]*Université de Franche-Comté, Institut UTINAM-UMR CNRS 6213, 25030 Besançon cedex, France*

[2]*Université de Rennes 1, Chimie et Ingénierie des Procédés - UMR 6226 CNRS (Sciences Chimiques de Rennes), 35042 Rennes cedex, France*

Abstract: Up to now, the SEDE (Steric Electric and Dielectric Exclusion) model was used to describe solute rejection in nanofiltration or membrane potential measurements. This model uses four fitting parameters: pore size, thickness to membrane porosity ratio, volume charge density (X) and dielectric constant of the solution inside pores (ε_p). Because these two latter parameters are extremely difficult to measure, an alternative method for assessing the SEDE model was to study both salt rejections and membrane potentials for a same salt. Experiments were conducted with a NF polyamide membrane in $CaCl_2$ solutions. In the case of single salt solutions, experimental rejections and membrane potentials can be described by a number of couples (X, ε_p) because both electric and dielectric exclusion contribute to reject ions. Only, one of the couples was found to provide a good description of both experimental rejections and membrane potentials. The fact that a unique choice for X and ε_p allows accounting simultaneously for both the salt rejection and the membrane potential data is an indicator of the global coherence of the SEDE model.

Keywords: Nanofiltration, Membrane potential, Salt rejection, Donnan exclusion, Dielectric exclusion.

INTRODUCTION

Among all the membrane separation processes in liquid phase, nanofiltration (NF) is one of the most recent and its applications are increasing. This membrane technology uses membranes with pore sizes in the nanometer range to meet industrial needs in the area of small molecules (< 1500 Da) and ions separation. Due to its real application potentialities for the separation or purification of liquid mixtures (industrial effluent treatment, production of drinking water…), the researchers' attention has been focussed to the development and optimization of mathematical models able to predict separation properties in NF. The most widely adopted NF models are based on the extended Nernst-Planck equation to describe the mass transfer and an equilibrium partitioning relation to describe the distribution of ions at the pore inlet and outlet. Among these continuous models, the so-called DSPM (Donnan-Steric partitioning Pore Model) developed by Bowen *et al.* [1] has been applied to analyze retention properties of a variety of NF membranes. However, the DSPM and other related models based on a steric/electric exclusion mechanism suffer from several weaknesses. Firstly, in many cases they are unable to fit experimental rejections of various electrolytes with a single value of the membrane thickness to membrane porosity ratio ($\Delta x/A_k$). Secondly, the Donnan exclusion theory fails to describe the high rejections observed with some NF membranes in the case of ionic solutions containing divalent counterions. Ten years ago, the SEDE (Steric Electric and Dielectric Exclusion) model including the dielectric exclusion mechanism (in terms of both Born dielectric effect and image forces contribution) in partitioning equations at membrane/solution interfaces was proposed [2]. Unlike the classical theory, this improved transport model was shown to provide a rather good description of the rejection properties of many membranes vis-à-vis single salt solutions and electrolyte mixtures [2-4] with physically realistic values of ε_p (*i.e*. ranging from 42 to 75). However, by including the dielectric exclusion mechanism into the classical theory, a new fitting parameter had to be then considered: the dielectric constant of the solution inside pores of the active layer. The measurement of this parameter is extremely difficult due the multilayer (thick support layers) and composite (membrane material and confined solution) structure of NF membranes. Also, the determination of the charge density within the skin-layer pores is complicated due to the multilayer structure of membranes [5-7] and their ion-selective properties [8-10]. An alternative method is to measure the streaming current along membrane skin-layers [11-13]. However, the external charge density estimated from tangential streaming current measurements may be very different from the charge density inside pores. It may provide only a rough estimate of the charge density within nanopores [3]. Because these two parameters, X and ε_p, are difficult to measure, a

*Address correspondence to this author at the Université de Franche-Comté, Institut UTINAM-UMR CNRS 6213, 25030 Besançon cedex, France;
Tel: +33 3 81 66 20 32;
E-mail: patrick.fievet@univ-fcomte.fr

E-ISSN: 2410-1869/16

possible alternative for assessing the SEDE model is to study not only solute rejection (as is often the case in recent NF modelling), but also the electric membrane potential. This potential is defined as the electrical potential difference arising through a membrane that separates two solutions of the same electrolyte at the same temperature and hydrostatic pressure but different concentrations. After applying the SEDE model to the study of salt rejection, its application was extended to investigating membrane potential [14-16]. The influence of the steric, electric and dielectric effects on this parameter was studied with binary and ternary electrolytes (*i.e.*, three different ions coming from two binary electrolytes with a common ion) [14-16]. In particular, it was shown that the Donnan and Born dielectric exclusions affect the membrane potential of charged membranes similarly; In other words, a number of pairs of X and ε_p values can lead to the same membrane potential value. As a result, neither the volume charge density nor the dielectric constant inside pores can be determined unambiguously by means of membrane potential experiments.

The aim of the present work is to carry out both rejection and membrane potential measurements in order to demonstrate that the experimental rejection and membrane potential can be well reproduced by using a unique choice for the four parameters of the model. Experiments were conducted with a NF polyamide membrane and $CaCl_2$ solutions at two pH values.

THEORY

Since the SEDE model has been described in details in previous works [2-4], just a brief presentation of the model is given below. All symbols are defined in the list of nomenclature section. The fitting parameters of the SEDE model are: the effective pore radius r_p, the effective thickness-to-porosity ratio ($\Delta x/A_k$), the effective volume charge density X (*i.e.*, the mole number of fixed charges per unit of pore volume) and the dielectric constant of the solution filling pores ε_p, both being considered constant through the membrane. Unlike the first two parameters, the other two depend on the physico-chemical properties of the surrounding solution. The superscript "int" stands for 0 or Δx depending on the interface that is considered and the bar refers to a magnitude inside the membrane.

Transport and Partitioning Equations

Within the scope of the SEDE model, the solute transfer is described as being the result of the following steps: first, a distribution of charged species at the membrane/feed solution interface resulting from size effects, Donnan exclusion and dielectric exclusion; secondly, a transport through the membrane by a combination of diffusion, migration and convection when a transmembrane pressure is applied (NF experiments) or by a combination of diffusion and migration when a concentration difference is applied on both sides of the membrane (membrane potential experiments), and thirdly, a redistribution of charged species at the second membrane/solution interface according to the same distribution laws as those at the first interface (Figure **1**).

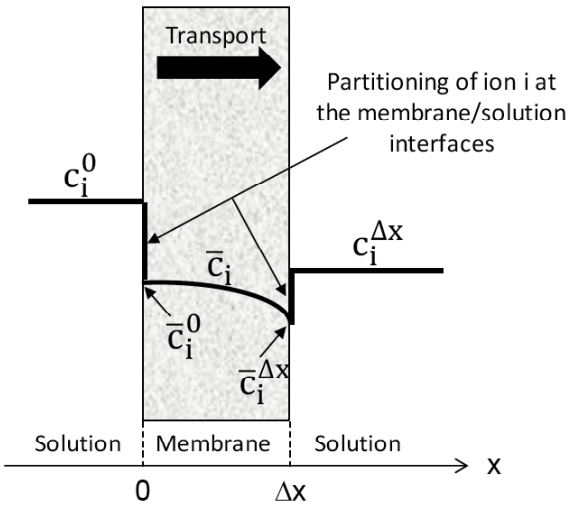

Figure 1: Schematic representation of the distribution of an ion i through the membrane. c_i and $\bar{c}_i$ are the concentrations of ion i outside and inside the membrane pores, respectively. The superscripts 0 and Δx denote the membrane/concentrated solution and membrane/diluted solution interfaces, respectively.

The governing equations of the model are collected in Tables **1** and **2**. The solute transport through the membrane is described by means of the extended Nernst–Planck equation that considers diffusion, electromigration (only for charged species ($z_i \neq 0$)) and convection (see Table **1**, Eq. (1)). In this work, the equations derived by Bungay and Brenner [17] were applied to calculate hindrance factors for the diffusion (Eq. (2)) and convection (Eq. (3)).

The distribution of ions at both membrane/external solution interfaces is described by Eq. (13) (see Table **2**), which is modified the Donnan relation including steric hindrance and dielectric exclusions ($\Gamma_i = \phi_i$ for uncharged species ($z_i = 0$)). Within the scope of the SEDE model, the Born effect is described by Eq. (14) which is the modified Born equation that considers the

Table 1: Transport Equations Used in the SEDE Model

Extended Nernst–Planck equation:

$$j_i = -K_{i,d} D_{i,\infty} \frac{d\overline{c}_i}{dx} - \frac{z_i \overline{c}_i K_{i,d} D_{i,\infty} F}{RT} \frac{d\overline{\psi}}{dx} + K_{i,c} \overline{c}_i V \quad (1)$$

with

$$K_{i,d} = \frac{6\pi}{K_{i,f}} \quad (2)$$

$$K_{i,c} = \frac{(2-\varphi_i) K_{i,s}}{2K_{i,f}} \quad (3)$$

$$K_{i,f} = \frac{9}{4}\pi^2\sqrt{2}(1-\lambda_i)^{-5/2}\left[1+\sum_{n=1}^{2} a_n (1-\lambda_i)^n\right] + \sum_{n=0}^{4} a_{n+3}\lambda_i^n \quad (4)$$

$$K_{i,s} = \frac{9}{4}\pi^2\sqrt{2}(1-\lambda_i)^{-5/2}\left[1+\sum_{n=1}^{2} b_n (1-\lambda_i)^n\right] + \sum_{n=0}^{4} b_{n+3}\lambda_i^n \quad (5)$$

$$\varphi_i = (1-\lambda_i)^2 \quad \text{(cylindrical pores)} \quad (6)$$

$$\lambda_i = r_{i,Stokes} / r_p \quad (7)$$

a_1 =-73/60, a_2 =77.293/50.400, a_3 =-22.5083, a_4 =-5.6117, a_5 =-0.3363, a_6 =-1.216, a_7 1.647, b_1 =7/60, b_2 =-2.227/50.400, b_3 =4.0180, b_4 =-3.9788, b_5 =-1.9215, b_6 =4.392, b_7. =5.006.

Relation between ionic molar flux j_i and permeate volume flux J_V:

$$j_i = V c_i^{\Delta x} = \frac{J_V c_i^{\Delta x}}{A_k} \quad (8)$$

Concentration gradients inside pores:

$$\frac{d\overline{c}_i}{dx} = \frac{J_V}{K_{i,d} D_{i,\infty} A_k}\left(K_{i,c}\overline{c}_i - c_i^{\Delta x}\right) - \frac{z_i F \overline{c}_i}{RT}\frac{d\overline{\psi}}{dx} \quad (9)$$

Zero electric current condition (steady state)

$$F\sum_i z_i j_i = 0 \quad (10)$$

Electrical potential gradient inside pores:

$$\frac{d\overline{\psi}}{dx} = \frac{-\sum_i z_i K_{i,d} D_{i,\infty}\frac{d\overline{c}_i}{dx} + \frac{J_V}{A_k}\sum_i z_i K_{i,c}\overline{c}_i}{\frac{F}{RT}\sum_i z_i^2 \overline{c}_i K_{i,d} D_{i,\infty}} \quad (11)$$

Electroneutrality condition inside pores:

$$\sum_i z_i \overline{c}_i + X = 0 \qquad \text{for } 0^+ \le x \le \Delta x^- \quad (12)$$

Table 2: Partitioning Equations Used in the SEDE Model

Partitioning equations at the membrane / solution interfaces:

$$\Gamma_i = \frac{\overline{c}_i^{\,\text{int}}}{c_i^{\,\text{int}}} = \varphi_i \exp\left(-\frac{z_i e \Delta\Psi_D^{\text{int}}}{k_B T}\right)\exp\left(-\Delta W_{i,Born}^{'}\right)\exp\left(-\Delta W_{i,image}^{'\,\text{int}}\right) \quad (13)$$

with

$$\Delta W_{i,Born}^{'} = \frac{(z_i e)^2}{8\pi \overset{o}{a}_0 k_B T r_{i,cav}}\left(\frac{1}{\varepsilon_p} - \frac{1}{\varepsilon_b}\right) \quad (14)$$

$$\Delta W_{i,image}^{'\,\text{int}} = \frac{2\alpha_i}{\pi}\int_0^{\infty} \frac{K_0(k)K_1(\nu) - \tilde{\beta}(k)K_0(\nu)K_1(k)}{I_1(\nu)K_0(k) + \tilde{\beta}(k)I_0(\nu)K_1(k)}\, dk \quad (15)$$

$$\alpha_i = \frac{(z_i e)^2}{8\pi \overset{o}{a}_0 \varepsilon_p k_B T r_p} \quad (16)$$

$$\nu = \sqrt{k^2 + \left(\mu^{\text{int}}\right)^2} \quad (17)$$

$$\mu^{\text{int}} = F\, r_p \sqrt{\frac{\sum_i z_i^2 c_i^{\,\text{int}} \varphi_i \exp\left(-\frac{z_i e}{k_B T}\Delta\Psi_D^{\text{int}} - \Delta W_{i,Born}^{'} - \Delta W_{i,image}^{'\,\text{int}}\right)}{RT\ \overset{o}{a}_0 \varepsilon_p}} \quad (18)$$

$$\beta^{\text{int}} = \frac{k}{\sqrt{k^2 + \left(\mu^{\text{int}}\right)^2}}\frac{\varepsilon_m}{\varepsilon_p} \quad (19)$$

radius of the cavity formed by the ion i in the solvent ($r_{i,cav}$). This latter was estimated according to the procedure proposed by Rashin and Honig [18]. The interaction between the ions and the induced polarization charges is described by Eq. (15) that was first derived by Yaroshchuk [19].

Rejection

The extended Nernst–Planck equation can be rewritten so as to establish the expression of the concentration gradient inside pores, *i.e.* for $0^+ \le x \le \Delta x^-$ (Eq. (9)). The expression of the electric potential gradient (Eq. (11)) is derived from Eq. (1) and the condition of zero electric current flowing through the membrane at the steady state (Eq. (10)). The electroneutrality condition inside pores is expressed by Eq. (12), Solving transport equations and partitioning equations allows computing the rejection of an ion i (see Table **3**, Eq. (20)).

Membrane Potential

Within the scope of the SEDE model, the membrane potential ($\Delta\Psi_m$) is the summation of the difference of the Donnan potentials at both interfaces, and the diffusion potential occurring through the membrane pores (Eq. (21)). A schematic representation of the membrane potential arising through the membrane is shown in Figure **2**.

Rearranging Eq. (13) yields the expression for the Donnan potential (Eq. 22). The volume flux resulting from the osmotic pressure gradient is assumed to be negligible and so, the contribution of convection is neglected in the extended Nernst–Planck equation throughout this work. Substituting Eq. (1) for both cations and anions in Eq. (10) and considering the derivative of Eq. (12) yields, after the integration between pore ends, the expression for the diffusion potential through the membrane pores (Eq. (24)). Substituting Eqs (22) and (24) in Eq. (21) yields the expression of the membrane potential. For a 2-1 electrolyte (such as $CaCl_2$) and a concentration ratio of

Table 3: Transport Parameters

Intrinsic rejection:

$$R_{i,\mathrm{int}} = 1 - \frac{c_i^{\Delta x}}{c_i^0} \quad (20)$$

Membrane potential:

$$\Delta\Psi_m = \Delta\Psi_D^{\Delta x} - \Delta\Psi_D^0 + \Delta\Psi_{diff} \quad (21)$$

Donnan Potential:

$$\Delta\Psi_D^{\mathrm{int}} = \overline{\psi}^{\mathrm{int}} - \psi^{\mathrm{int}} = \frac{RT}{z_i F}\ln\left(\frac{\kappa_i^{\mathrm{int}} c_i^{\mathrm{int}}}{\overline{c}_i^{\mathrm{int}}}\right) \quad (22)$$

with

$$\kappa_i^{\mathrm{int}} = \varphi_i \exp\left(-\Delta W_{i,Born}^{\mathrm{int}}\right)\exp\left(-\Delta W_{i,image}^{\mathrm{int}}\right) \quad (23)$$

$$\Delta\Psi_{diff} = -\frac{k_B T}{z_i e}\left(\frac{K_{+,d}D_+ - K_{-,d}D_-}{z_+ K_{+,d}D_+ - z_- K_{-,d}D_-}\right)\ln\left(\frac{z_+^2 K_{+,d}D_+ \overline{c}_+^0 + z_-^2 K_{-,d}D_- \overline{c}_-^0}{z_+^2 K_{+,d}D_+ \overline{c}_+^{\Delta x} + z_-^2 K_{-,d}D_- \overline{c}_-^{\Delta x}}\right) \quad (24)$$

Membrane potential for a 2-1 asymmetric electrolyte and $c_i^0 = 2c_i^{\Delta x}$:

$$\Delta\Psi_m = \frac{k_B T}{z_i e}\ln\left(\frac{\kappa_i^{\Delta x}\overline{c}_i^0}{2\overline{c}_i^{\Delta x}\kappa_i^0}\right) - \frac{k_B T}{e}\left(\frac{K_{+,d}D_+ - K_{-,d}D_-}{2K_{+,d}D_+ + K_{-,d}D_-}\right)\ln\left(\frac{4K_{+,d}D_+\overline{c}_+^0 + K_{-,d}D_-\overline{c}_-^0}{4K_{+,d}D_+\overline{c}_+^{\Delta x} + K_{-,d}D_-\overline{c}_-^{\Delta x}}\right) \quad (25)$$

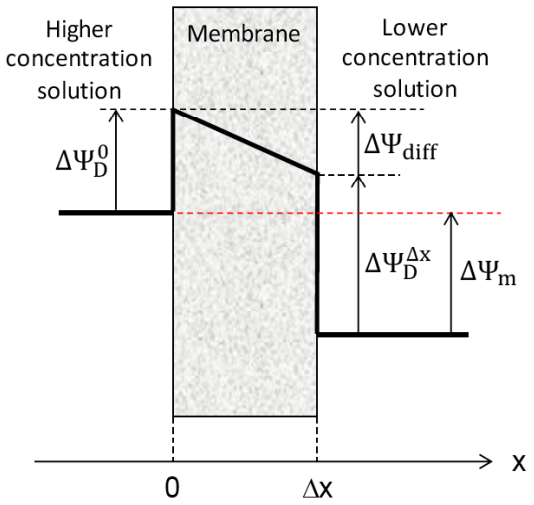

Figure 2: Schematic representation of the membrane potential ($\Delta\Psi_m$) arising through the membrane. $\Delta\Psi_D$: Donnan potential; $\Delta\Psi_{diff}$: diffusion potential.

2 (*i.e.* $c_i^0 = 2c_i^{\Delta x}$), the expression of the membrane potential is given by Eq. (25). For all calculations, the diffusion coefficients of calcium and chloride ions were set at 0.792 and 2.031 10^{-9} m^2 s^{-1}, respectively.

EXPERIMENTAL

Membrane and Chemicals

The membrane studied in this work is a tubular polyamide membrane (AFC 30) supplied by PCI Membrane System (Whiteley, United Kingdom), with a filtration area of 0.022 m^2 and a hydraulic radius of 1.2 cm. The salt used was $CaCl_2$ of pure analytical grade supplied by Fisher Scientific. Salt solutions were prepared with demineralised water (conductivity < 1µS cm^{-1}). The pH of the various solutions was adjusted at 6.2 and 7.6 with KOH.

Membrane Potential

The test cell used for membrane potential measurements is composed of two polycarbonate half-cells of volume 20 cm^3 and the membrane is clamped between them by using silicone rubber rings [16]. Fluids in both compartments are stirred vigorously, at the same speed, by a magnetic stirrer in order to minimize concentration polarization at the membrane surfaces. The exposed membrane area was of 12.6 cm^2. Solutions at various concentrations were used but the concentration ratio between the two compartments was maintained at a constant value of 2. Concentrations were 0.30 and 1.15 mol m^{-3} for the lower concentration solutions.

The tubular membrane was cut lengthwise and the "effective layer" of the membrane (active layer + part of support layer) was peeled off the supporting fabric. Before each measurement the membrane was permeated with the lower concentration solution during 2 days. For the whole study, the active layer of the membrane was put in contact with the higher concentration solution. The membrane potential (defined as the difference between the potential in bulk solution of higher concentration and the potential in bulk solution of lower concentration) was determined by inserting two Ag/AgCl electrodes (connected to a voltmeter) directly into the bulk solutions. In order to cancel the effect of the asymmetry potential, the potential difference was measured by interchanging the electrodes in the two compartments and the average of the two measurements was taken for the cell potential. The asymmetry potential was not greater than 0.2 mV. The electrode inserted into solution of lower concentration was grounded. The membrane potential $\Delta\Psi_m$ was obtained by subtracting the concentration potential (the value of which is $\frac{RT}{F}\ln 2 = 17.8$ mV), resulting from different concentrations of solutions, from the measured cell potential. Measurements were repeated three times.

Ion Rejection

The experimental set-up can be found elsewhere [20]. From a feed container (25 L), a centrifugal pump allows the solution to circulate into the transversal

filtration module. Experimental conditions were as follows: temperature, 25 °C, feed cross-flow rate, 0.4-0.5 m^3 h^{-1}, transmembrane pressure 5-30 bar. The permeate was recycled to maintain a constant concentration in the feed tank. Feed and permeate concentrations were determined from conductivity measurements. The permeate volume flux was obtained by weighing the fluid amount flowing through the membrane. The effect of concentration polarization was taken into account by using a mass transfer coefficient, obtained by the semi-empirical equation of Dittus and Boelter [21]. The equations used for calculating the intrinsic rejections ($R_{i,\text{int}}$) are collected in Table **4**.

Table 4: Equations used for Calculating the Intrinsic Rejection

Intrinsic rejection:

$$R_{i,\text{int}} = \frac{R_{i,obs}\exp\left(J_v/k\right)}{1-R_{i,obs}\left(1-\exp\left(J_v/k\right)\right)} \quad (26)$$

Observed rejection:

$$R_{i,obs} = 1-\frac{c_i^{\Delta x}}{c_i^f} \quad (27)$$

Mass-transfer coefficient k in the polarisation layer:

$$k = \frac{D_{salt}}{\delta} \quad (28)$$

with

$$D_{salt} = \frac{\left(|z_+| + |z_+|\right) D_+ D_+}{|z_+| D_+ + |z_+| D_+} \quad (29)$$

Sherwood correlation:

$$Sh = \frac{k' d_h}{D_{salt}} = 0.04\,\text{Re}^{0.75}\,Sc^{0.33} \quad (30)$$

RESULTS

As said previously, the SEDE model is a four-parameter model. In the present work, the volume charge density of the membrane (X) and the dielectric constant of the solution inside the membrane pores (ε_p) were estimated using the following procedure. Firstly, the membrane effective pore radius (r_p) and thickness-to-porosity ratio ($\Delta x/A_k$) of the active layer were assessed from glucose rejection as a function of permeate volume flux (Figure **3**). Values of 0.53 nm and 1.72 µm were obtained for r_p and $\Delta x/A_k$, respectively. These values are in good agreement with those obtained by Bouranene *et al.*: r_p = 0.55 nm and $\Delta x/A_k$ = 2.43 µm [22]. The dielectric constant of the membrane ε_m was fixed at 3, according to available data for polyamide material [23] and the bulk solution dielectric constant ε_b was set at 78.54. Thus, the two single fitting parameters were ε_p and X.

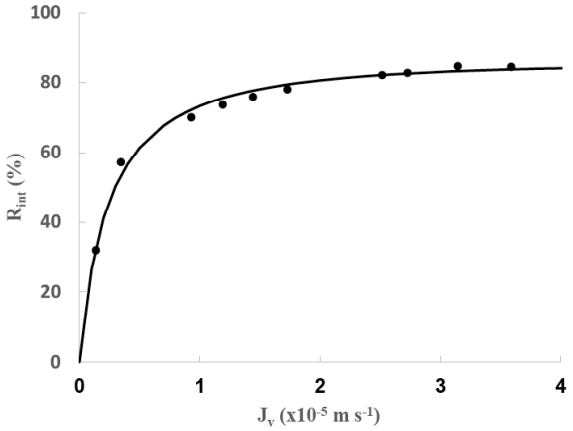

Figure 3: Intrinsic rejection of glucose vs permeate volume flux; Glucose solution at 2 g L^{-1}; calculations of R_{int} were performed by considering $D_{glucose,\infty}$ = 6.9x10^{-10} m^2 s^{-1} [1].

Figure **4** shows the variation of the normalized membrane potential ($\Delta\Psi_m$ is scaled on kT) with the salt concentration of the diluted compartment at pH of 6.2 and 7.6. It must be remembered that each data represent the mean value calculated from three measurements. A standard deviation of about ± 0.2 mV was obtained at various concentrations and pH. As can be seen, the membrane potential slightly increases with salt concentration. This increase can be due to a lower Donnan exclusion resulting from a stronger screening of the membrane fixed charge with increasing salt concentration [24] and/or to lower dielectric effects via the contribution of image forces. Indeed, image forces become weaker as the electrolyte concentration increases due to a stronger screening of the interaction between the ions and their images, yielding to higher membrane potential [2].

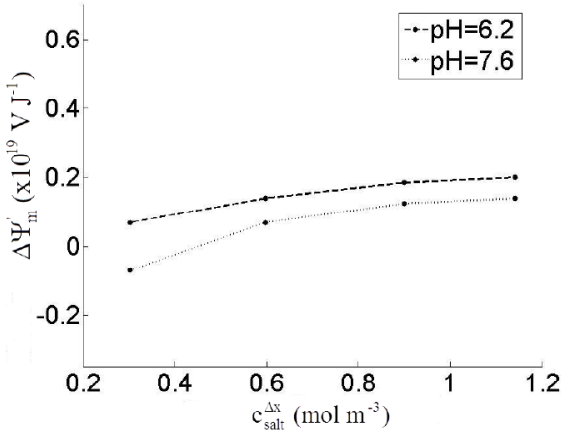

Figure 4: Normalized experimental membrane potential ($\Delta\Psi'_m = \frac{\Delta\Psi_m}{k_B T}$) vs the concentration of the most diluted compartment ($c_{salt}^{\Delta x}$) at two pH values (6.2 and 7.6). $CaCl_2$ salt.

In a previous work [14], it was shown that an increase in X, in absolute value, (neglecting the dielectric effects) or a decrease in ε_p (neglecting the image forces contribution) shifts the potential-concentration curve towards higher salt concentrations. Indeed, when X is increased or ε_p decreased, more counter-ions are required to screen the fixed charge of a more strongly charged membrane. Since the same qualitative effect is produced on the membrane potential by decreasing ε_p or increasing X, it means that there are different couples of values (X, ε_p) that lead to the same membrane potential value. A set of (X, ε_p) values leading to identical membrane potential values (variation of ± 0.1 mV) is plotted in Figure **5** for illustration purpose. By considering that ε_p is comprised between 50 and the bulk dielectric constant (78.54) (these values appear to be physically realistic), several couples (X, ε_p) were then determined for each concentration and pH. In order to determine true values of X and ε_p, the different couples of values (X, ε_p) deduced from membrane potential measurements were then used to compute rejections versus permeate volume flux by setting the feed concentration equals to the diluted side concentration used for membrane potential experiments. The couple of values (X, ε_p) leading to the best fit of the experimental rejections was then chosen (Figure **6**). Best fits were determined by means of the least-squares fitting objective function (S_y) defined for n data points as follows:

$$S_y = \left[\frac{\sum_{j=1}^{n} \left(R_{i,\exp} - R_{i,calc} \right)^2}{n-1} \right]^{0.5} \quad (26)$$

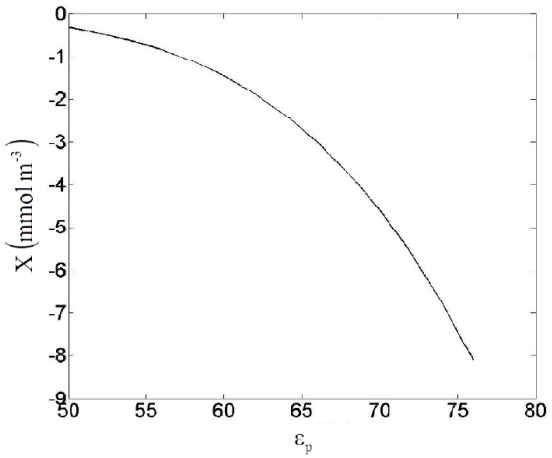

Figure 5: Set of couples (ε_p, X) leading to the same membrane potential value measured at $c_{salt}^{\Delta x}$ = 0.30 mol m^{-3}. $CaCl_2$ salt; pH = 6.2. r_p = 0.53 nm and ε_m = 3.

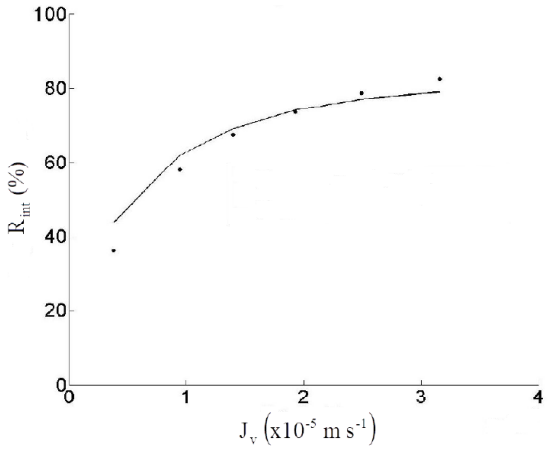

Figure 6: Comparison between theoretical (lines) and experimental rejections (symbols). 0.30 mol m^{-3} $CaCl_2$; pH = 6.2. r_p = 0.53 nm, ε_m = 3, ε_p = 70, X = -4.6 mmol m^{-3}.

The fact that a unique choice for X and ε_p (with the same pore radius and thickness-to-porosity ratio) allows accounting simultaneously for both the membrane potential and salt rejection data is an indicator of the global coherence of the SEDE transport model.

For each experimental conditions, the couples providing best fits (X, ε_p) are reported in Table **5**. Firstly, it appears that the polyamide membrane is negatively charged, which is in agreement with reported studies dealing with polyamide membranes. However, the charge density is found to be very low in $CaCl_2$ solutions at concentrations and pH under consideration. A preferential adsorption of Ca^{2+} ions on the membrane surface, which could be caused prevailingly by site-binding effects on the negatively charged sites of the membrane, could explain this result [25,26].

Table 5: Couples (ε_p, X) for the Reproduction of Both Experimental Rejections and Membrane Potential at Two Concentrations (0.30 and 1.15 mol m^{-3}) and pH (6.2 and 7.6)

$CaCl_2$ concentration (mol m^{-3})	0.30	0.30	1.15	1.15
pH	6.2	7.6	6.2	7.6
$\Delta\Psi_m$ (mV)	2.5	-2.8	7.9	5.4
ε_p	70	68	72	72
X (mmol m^{-3})	-4.60	-7.19	-10.4	-15.6

The normalized volume charge density $|X|/C_{salt}$, which is the parameter responsible for the Donnan electric exclusion, is about 0.01. It means that the

Donnan effect plays a minor role in the ion exclusion from pores [24]. Secondly, ε_p values are found to be smaller than the bulk value, ε_b, fixed at 78.54. These values, around 70, are in accordance with those reported in the literature, which are in the range of 42-75 depending on the nature of the membrane, the pore radius and the electrolyte type [2-4, 16, 27-32]. The decrease of the dielectric constant inside pores as compared with that of the external solution is usually attributed to the effects of both confinement and electric field generated by ionized surface sites [3]. Both effects are expected to produce an ordering of solvent dipoles. This ordered structure is thought to reduce the ability of the solvent molecules to respond to an external electric field and hence to reduce the medium dielectric constant. This has been confirmed by molecular dynamics simulations although some contradictory results do exist in the literature [33,34]. The membrane being very little charged, it can be concluded that the lowering of the dielectric constant of the solution inside pores originates only from confinement effect.

CONCLUSION

Up to now, the SEDE transport model was used to study either solute rejection or membrane potential. In the present work, the model was applied to simultaneously investigate the two transport parameters. It was shown that these experimental magnitudes can be well reproduced by using a unique choice for membrane pore size, thickness-to-porosity ratio, the volume charge density and the dielectric constant of the solution inside pores. This result is a proof of the global coherence of the SEDE model since it is able to describe two different transport parameters. This work again confirms that dielectric exclusion phenomena may play an important role in the separation properties of NF membranes.

NOMENCLATURE

A_k: Porosity of the membrane active layer (-)

$\overline{c}_i$: Concentration inside the membrane pores (mol m^{-3})

$\overline{c}_i^{int}$: Concentration just inside the membrane pores, at the membrane/external solution interface (mol m^{-3})

c_i^f : Feed concentration of ion i (mol m^{-3})

c_i^{int} : Concentration just outside the membrane, at the membrane/external solution interface (mol m^{-3})

c_{salt}^{int} : Salt concentration just outside the membrane, at the membrane/external solution interface (mol m^{-3})

d_h: Hydraulic diameter (m)

D_i: Bulk diffusion coefficient of ion i (m^2 s^{-1})

D_{salt}: Effective diffusivity of the salt (m^2 s^{-1})

e: Elementary charge; 1.602177x10^{-19} C

F: Faraday constant; 96485 C mol^{-1}

I_0: Modified Bessel function (-)

I_1: Modified Bessel function (-)

j_i: Molar flux density of ion i (mol m^{-2} s^{-1})

J_V: Permeate volume flux (m s^{-1})

k': Mass-transfer coefficient in the polarization layer (m s^{-1})

k: Wave vector (-)

k_B: Boltzmann constant; 1.38066x10^{-23} J K^{-1}

K_0: Modified Bessel function (-)

K_1: Modified Bessel function (-)

$K_{i,c}$: Hydrodynamic coefficient accounting for the effect of pore walls on convective transport for ion i (-)

$K_{i,d}$: Hydrodynamic coefficient for hindered diffusion inside pores for ion i (-)

$K_{i,s}$: Hydrodynamics function for ion i (-)

$K_{i,t}$: Hydrodynamics function for ion i (-)

r_p: Pore radius (m)

$r_{i,cav}$: Cavity radius of ion *i* (m)

$r_{i,Stokes}$: Stokes radius of solute i (m)

R: Ideal gas constant; 8.314 J $mol^{-1}K^{-1}$

Re: Reynolds number (-)

$R_{i,int}$: Intrinsic rejection for ion i (-)

$R_{i,obs}$: Observed rejection for ion i (-)

Sc: Schmidt number (-)

Sh: Sherwood number (-)

T: Temperature (K)

V: Fluid velocity inside pores (m s^{-1})

x: Coordinate (m)

X: Volume charge density of the membrane active layer (mol m^{-3})

z_i: Charge number of ion i (-)

Greek symbols

δ: Thickness of the polarization layer (m)

$\Delta W'_{i,Born}$: Dimensionless excess solvation energy due to Born effect for ion i (-)

$\Delta W'^{int}_{i,image}$: Dimensionless excess solvation energy due to "image charges" for ion i (-)

Δx: Effective thickness of the active layer (m)

$\Delta\Psi_{diff}$: Diffusion potential (V)

$\Delta\Psi^0_D$: Donnan potential at the membrane/concentrated solution interface (V)

$\Delta\Psi^{\Delta x}_D$: Donnan potential at the membrane/diluted solution interface (V)

$\Delta\Psi_m$: Membrane potential (V)

$\Delta\Psi'_m$: Normalised Membrane potential ($\Delta\Psi'_m = \Delta\Psi_m / k_B T$) (V J^{-1})

ε_0: Vacuum permittivity; 8.85419x10^{-12} (F m^{-1})

ε_b: Dielectric constant of the bulk solution outside pores (-)

ε_m: Dielectric constant of the membrane active layer (-)

ε_p: Effective dielectric constant inside pores (-)

ϕ_i: Steric partitioning coefficient for ion i (-)

Γ_i : Partitioning coefficient for ion i (-)

κ_i^{int} : Steric-Dielectric partitioning coefficient for ion i (-)

λ_i: Ratio of the Stokes radius of solute i to the pore radius (-)

μ: Effective dimensionless reciprocal screening length for interaction between ions and induced polarization charges (-)

$\overline{\Psi}$: Local electrical potential inside pores (V)

Ψ^{int} : Local electrical potential just outside of the membrane, at the membrane/external solution interface (-)

$\overline{\Psi}^{int}$: Local electrical potential just inside the membrane pores, at the membrane/external solution interface (-)

Superscript

f: Feed

int: Membrane/external solution interface

Δx: Membrane/diluted solution interface

0: Membrane/concentrated solution interface

Subscript

i: Ion i

int: Intrinsic

obs: Observed

REFERENCES

[1] Bowen WR, Mohammad AW, Hilal N. Characterisation of nanofiltration membranes for predictive purposes - use of salts, uncharged solutes and atomic force microscopy. J Membr Sci 1997; 126: 91-105. http://dx.doi.org/10.1016/S0376-7388(96)00276-1

[2] Szymczyk A, Fievet P. Investigating transport properties of nanofiltration membranes by means of a steric, electric and dielectric exclusion model. J Membr Sci 2005; 252: 77-88. http://dx.doi.org/10.1016/j.memsci.2004.12.002

[3] Szymczyk A, Sbai M, Fievet P, Vidonne A. Transport properties and electrokinetic characterization of an amphoteric nanofilter. Langmuir 2006; 22: 3910-3919. http://dx.doi.org/10.1021/la051888d

[4] Szymczyk A, Fatin-Rouge N, Fievet P, Ramseyer C, Vidonne A. Identification of dielectric effects in nanofiltration of metallic salts. J Membr Sci 2007; 287: 102-110. http://dx.doi.org/10.1016/j.memsci.2006.10.025

[5] Szymczyk A, Fievet P, Reggiani JC, Pagetti J. Desalination 1998; 116: 81-88. http://dx.doi.org/10.1016/S0011-9164(98)00059-9

[6] Labbez C, Fievet P, Szymczyk A, Aoubiza B, Vidonne A, Pagetti J. Theoretical study of the electrokinetic and electrochemical behaviors of two-layer composite membranes J Membr Sci 2001; 184: 79-95. http://dx.doi.org/10.1016/S0376-7388(00)00611-6

[7] Szymczyk A, Labbez C, Fievet P, Aoubiza B, Simon C. Streaming potential through multilayer membranes. AIChE 2001; 474: 2349-2358. http://dx.doi.org/10.1002/aic.690471019

[8] Benavente J, Jonsson G. Electrokinetic characterization of composite membranes: estimation of different electrical contributions in pressure induced potential measured across reverse osmosis membranes. J Membr Sci 2000; 172: 189-197. http://dx.doi.org/10.1016/S0376-7388(00)00325-2

[9] Canas A, Ariza MJ, Benavente J. Characterization of active and porous sublayers of a composite reverse osmosis membrane by impedance spectroscopy, streaming potential and membrane potentials, salt diffusion and X-ray photoelectron spectroscopy measurements. J Membr Sci 2001; 183: 135-146. http://dx.doi.org/10.1016/S0376-7388(00)00583-4

[10] Yaroshchuk AE, Boiko YP, Makovetskiy AL. Filtration potential across membranes containing selective layers. Langmuir 2002; 18(10): 5154-5162. http://dx.doi.org/10.1021/la025503s

[11] Déon S, Fievet P, Osman Doubad C. Tangential streaming potential/current measurements for the characterization of composite membranes. J Membr Sci 2012; 423-424: 413-421. http://dx.doi.org/10.1016/j.memsci.2012.08.038

[12] Idil Mouhoumed E, Szymczyk A, Schäfer A, Paugam L, La YH. Physico-chemical characterization of polyamide NF/RO membranes:Insight from streaming current measurements. J Membr Sci 2014; 461: 130-138. http://dx.doi.org/10.1016/j.memsci.2014.03.025

[13] Efligenir A, Fievet P, Déon S, Sauvade P. Tangential electrokinetic characterization of hollow fiber membranes: Effects of external solution on cell electric conductance and streaming current. J Membr Sci 2015; 496: 293-300. http://dx.doi.org/10.1016/j.memsci.2015.09.002

[14] Lanteri Y, Szymczyk A, Fievet P. Influence of Steric, Electric, and Dielectric Effects on Membrane Potential. Langmuir 2008; 24(15): 7955-7962. http://dx.doi.org/10.1021/la800677q

[15] Lanteri Y, Szymczyk A, Fievet P. Membrane Potential in Multi-Ionic Mixtures. J Phys Chem B 2009; 113: 9197-9204. http://dx.doi.org/10.1021/jp901110c

[16] Escoda A, Lanteri Y, Fievet P, Déon S, Szymczyk A. Determining the dielectric constant inside pores of nanofiltration membranes from membrane potential measurements. Langmuir 2010; 26(18): 14628-14635. http://dx.doi.org/10.1021/la1023949

[17] Bungay PM, Brenner H. Int. The motion of a closely fitting sphere in a fluid-filled tube. J Multiphase Flow 1973; 1: 25-56. http://dx.doi.org/10.1016/0301-9322(73)90003-7

[18] Rashin AA, Honig B. Reevaluation of the Born model of ionic hydration. J Phys Chem 1985; 89: 5588-5593. http://dx.doi.org/10.1021/j100272a006

[19] Yaroshchuk AE. Non-steric mechanisms of nanofiltration: superposition of Donnan and dielectric exclusion. Sep Purif Technol 2001; 22-23: 143-158. http://dx.doi.org/10.1016/S1383-5866(00)00159-3

[20] Labbez C, Fievet P, Szymczyk A, Vidonne A, Foissy A, Pagetti J. Retention of mineral salts by a polyamide nanofiltration membrane. Sep Purif Technol 2003; 30: 47-55. http://dx.doi.org/10.1016/S1383-5866(02)00107-7

[21] Schweitzer PA. Handbook of Separations Techniques for Chemical Engineers, McGraw-Hill, New York; 1988.

[22] Bouranene S, Fievet P, Szymczyk A, El-Hadi Samar M., Vidonne A. Influence of operating conditions on the rejection of cobalt and lead ions in aqueous solutions by a nanofiltration polyamide membrane. J Membr Sci 2008; 325: 150-157. http://dx.doi.org/10.1016/j.memsci.2008.07.018

[23] Weast RC (Ed). Handbook of Chemistry and Physics, CRC Press, Boca Raton, FL; 1980.

[24] Palmeri J, Blanc P, Larbot A, David P. Theory of pressure-driven transport of neutral solutes and ions in porous ceramic nanofiltration membranes. J Membr Sci 1999; 160: 141-170. http://dx.doi.org/10.1016/S0376-7388(99)00081-2

[25] Teixeira MR, Rosa MJ, Nystrom M. The role of membrane charge in nanofiltration performance. J Membr Sci 2005; 265: 160-166. http://dx.doi.org/10.1016/j.memsci.2005.04.046

[26] Mazzoni C, Bandini S. On nanofiltration Desal-5 DK performances with calcium chloride–water solutions. Sep Purif Technol 2006; 52: 232–240. http://dx.doi.org/10.1016/j.seppur.2006.04.004

[27] Déon S, Dutournié P, Bourseau P. Modeling Nanofiltration with Nernst-Planck Approach and Polarization Layer. AIChE 2007; 53: 1952-1969. http://dx.doi.org/10.1002/aic.11207

[28] Escoda A, Déon S, Fievet P. Assessment of dielectric contribution in the modeling of multi ionic transport through nanofiltration membranes. J Membr Sci 2011; 378: 214-223. http://dx.doi.org/10.1016/j.memsci.2011.05.004

[29] Déon S, Dutournié P, Limousy L, Bourseau P, Transport of salt mixtures through nanofiltration membranes: Numerical identification of electric and dielectric contributions. Sep Purif Technol 2009; 69: 225-233. http://dx.doi.org/10.1016/j.seppur.2009.07.022

[30] Cavaco Morão AI, Szymczyk A, Fievet P, Brites Alves AM. Modelling the separation by nanofiltration of a multi-ionic solution relevant to an industrial process. J Membr Sci 2008; 322: 320-330. http://dx.doi.org/10.1016/j.memsci.2008.06.003

[31] Déon S, Escoda A, Fievet P, Dutournié P, Bourseau P. How to use a multi-ionic transport model to fully predict rejection of mineral salts by nanofiltration membranes. Chemical Engineering Journal 2012; 189-190: 24-31. http://dx.doi.org/10.1016/j.cej.2012.02.014

[32] Bouranene S, Fievet P, Szymczyk A. Investigating nanofiltration of multi-ionic solutions using the Steric, Electric and Dielectric Exclusion model. Chemical Engineering Science 2009; 64: 3789-3798. http://dx.doi.org/10.1016/j.ces.2009.05.020

[33] Senapati S, Chandra A. Dielectric constant of water confined in a nanocavity. J Phys Chem B 2001; 105: 5106-5109 http://dx.doi.org/10.1021/jp011058i

[34] Ballenegger, V, Hansen JP. Dielectric permittivity profiles of confined polar fluids. J Chem Phys 2005; 122(11): 11471. http://dx.doi.org/10.1063/1.1845431

Received on 02-05-2016 Accepted on 27-05-2016 Published on 31-05-2016

http://dx.doi.org/10.15379/2410-1869.2016.03.01.04